



# Cerebrovascular G<sub>i</sub> Proteins Protect Against Brain Hypoperfusion and Collateral Failure in Cerebral Ischemia

Salvador Castaneda-Vega<sup>1,2</sup>  · Sandra Beer-Hammer<sup>3,4</sup> · Veronika Leiss<sup>3</sup> · Hanna Napieczyńska<sup>1</sup> · Marta Vuozzo<sup>1</sup> · Andreas M. Schmid<sup>1</sup> · Hang Zeng<sup>5</sup> · Yi He<sup>5</sup> · Ursula Kohlhofer<sup>6</sup> · Irene Gonzalez-Menendez<sup>4,6</sup> · Leticia Quintanilla-Martinez<sup>4,6</sup> · Johann-Martin Hempel<sup>7</sup> · Maik Gollasch<sup>8,9</sup> · Xin Yu<sup>5,10</sup> · Bernd J. Pichler<sup>1,4</sup> · Bernd Nürnberg<sup>3</sup> 

Received: 18 April 2022 / Revised: 23 June 2022 / Accepted: 2 August 2022 / Published online: 8 September 2022  
© The Author(s) 2022

## Abstract

Cerebral hypoperfusion and vascular dysfunction are closely related to common risk factors for ischemic stroke such as hypertension, dyslipidemia, diabetes, and smoking. The role of inhibitory G protein-dependent receptor (G<sub>i</sub>PCR) signaling in regulating cerebrovascular functions remains largely elusive. We examined the importance of G<sub>i</sub>PCR signaling in cerebral blood flow (CBF) and its stability after sudden interruption using various *in vivo* high-resolution magnetic resonance imaging techniques. To this end, we induced a functional knockout of G<sub>i</sub>PCR signaling in the brain vasculature by injection of pertussis toxin (PTX). Our results show that PTX induced global brain hypoperfusion and microvascular collapse. When PTX-pretreated animals underwent transient unilateral occlusion of one common carotid artery, CBF was disrupted in the ipsilateral hemisphere resulting in the collapse of the cortically penetrating microvessels. In addition, pronounced stroke features in the affected brain regions appeared in both MRI and histological examination. Our findings suggest an impact of cerebrovascular G<sub>i</sub>PCR signaling in the maintenance of CBF, which may be useful for novel pharmacotherapeutic approaches to prevent and treat cerebrovascular dysfunction and stroke.

**Keywords** Ischemic stroke · MRI · Pertussis toxin · G protein · Cerebral microvessels

---

✉ Bernd J. Pichler  
Bernd.pichler@med.uni-tuebingen.de

✉ Bernd Nürnberg  
Bernd.nuernberg@uni-tuebingen.de

<sup>1</sup> Werner Siemens Imaging Center, Department of Preclinical Imaging and Radiopharmacy, Eberhard Karls University Tübingen and University Clinic, Tübingen, Germany

<sup>2</sup> Department of Nuclear Medicine and Clinical Molecular Imaging, Eberhard Karls University Tübingen and University Clinic, Tübingen, Germany

<sup>3</sup> Department of Pharmacology, Experimental Therapy and Toxicology, and Interfaculty Center for Pharmacogenomics and Drug Research, Eberhard Karls University Tübingen and University Clinic, Tübingen, Germany

<sup>4</sup> Cluster of Excellence iFIT (EXC 2180) “Image-Guided and Functionally Instructed Tumor Therapies”, Eberhard Karls University Tübingen and University Clinic, Tübingen, Germany

<sup>5</sup> High Field Magnetic Resonance Department, Max Planck Institute for Biological Cybernetics, Tübingen, Germany

<sup>6</sup> Institute of Pathology and Neuropathology, Eberhard Karls University and Comprehensive Cancer Center, Eberhard Karls University Tübingen and University Clinic, Tübingen, Germany

<sup>7</sup> Department of Diagnostic and Interventional Neuroradiology, Eberhard Karls University Tübingen and University Clinic, Tübingen, Germany

<sup>8</sup> Experimental and Clinical Research Center (ECRC), A Joint Cooperation Between the Charité Medical Faculty and the Max Delbrück Center for Molecular Medicine in the Helmholtz Association (MDC), Berlin, Germany

<sup>9</sup> Department of Internal and Geriatric Medicine, University – Medicine Greifswald, Greifswald, Germany

<sup>10</sup> Athinoula A. Martinos Center for Biomedical Imaging, Massachusetts General Hospital and Harvard Medical School, Charlestown, MA, USA

## Introduction

G<sub>i</sub> proteins are the principal signal transducers of a broad subset of G protein-coupled receptors (termed G<sub>i</sub>PCRs), including those for acetylcholine, adenosine, and catecholamines that control blood circulation [1–5]. In spite of many studies, the functions of G<sub>i</sub> protein-dependent signaling in the brain vasculature have been largely ignored. One major reason for the undefined role of G<sub>i</sub> proteins may be the lack of appropriate animal models, since a simultaneous genetic ablation of the major G<sub>α</sub> isoforms (G<sub>α</sub><sub>12</sub> and G<sub>α</sub><sub>13</sub>) produces embryonic lethality in mice [6]. On the other hand, the significance of singular knockouts is limited by overlapping functions of these isoforms. Pertussis toxin (PTX) has been used to study G<sub>i</sub> protein signaling in the cardiovascular system [7, 8], but the effects on cerebrovasculature have not yet been elucidated.

*In vivo*, PTX irreversibly and with high specificity blocks G<sub>i</sub>-linked GPCR signal transduction — hereafter referred to as non-cerebral G<sub>i</sub>PCR KO — by catalyzing covalent modification of a C-terminal cysteine residue of cellular G<sub>α</sub> isoforms [9–11]. In arteries and microvessels, PTX inhibits endothelium-dependent relaxation to certain agonists such as β-adrenergic ligands, angiotensin, serotonin, or relaxins and is therefore useful for the study of vasculopathies [2, 7, 8, 12–18]. We have previously demonstrated that PTX, administered in a single peritoneal injection, does not cross the blood–brain barrier (BBB) and does not modify G<sub>i</sub>PCR signaling in neurons [19]. PTX administration, however, still irreversibly interrupts G<sub>i</sub>PCR signaling for up to 96 h in cells outside of the CNS, including brain vasculature. Using PTX, in this work, we evaluate the effects in cerebral blood flow caused by permanent G<sub>i</sub>PCR modification of cells outside of the brain.

MRI provides a powerful set of neuroimaging tools that allow quantification of pathological changes at the functional level in the brain [20–22]. *In vivo* MRI allows consistent acquisition of multiple tissue characteristics in a single session permitting evaluation of their longitudinal development [20, 22].

In the present study, we focused, first, on the effects of PTX administration in systemic blood flow, cerebral blood flow (CBF), and microvascular patency and, second, on G<sub>i</sub>PCR-dependent vascular responses after acute vascular occlusion. Our data reveal that injection of PTX severely reduces cerebral perfusion and impedes compensatory mechanisms regulating CBF. As a result, microcirculation collapses during vascular occlusion, contributing to ischemic brain lesions.

## Materials and Methods

### Animal Experiments

The study was carried out in compliance with the ARRIVE guidelines. All experiments were performed according to the

EU Animals Scientific Procedures Act and the German law for the welfare of animals and were approved by the local animal ethical committees (Regierungspräsidium Tübingen, PH 10/13, PH 1/11, PH 04/19). C57BL/6 female, 8-week-old, mice were kept under specified pathogen-free conditions, controlled temperature, and humidity in 12-h day/night light cycles, receiving food and water ad libitum. Workflows of all experiments are sketched in the corresponding figures. We induced non-cerebral G<sub>i</sub>PCR KO using a single dose of PTX (150 μg/kg body weight) (Merck, Darmstadt, Germany) 48 h before intervention (sham or surgery), as previously shown [19, 23, 24]. Details are provided in the “Supplementary Information.”

### Whole-Body Semi-quantitative Perfusion

In order to determine whether PTX produced whole-body systemic organ-perfusion changes, mice weighing 20–23 g were evaluated using dynamic contrast-enhanced (DCE) MRI. Vehicle (phosphate-buffered solution, PBS) or PTX was injected intraperitoneal (i.p.) into 5 mice per group. After 48 h, transversal DCE images focusing on multiple body regions including the lung, kidney, paravertebral muscle, abdominal vessels, heart, and brain were acquired. Details are provided in the “Supplementary Information.”

### Longitudinal Multiparametric MRI—Animals and Treatment

For these experiments, 8-week-old mice were divided into four groups: PBS-pretreated sham-operated, PTX-pretreated sham-operated, PBS-pretreated occluded, and PTX-pretreated occluded. These groups were studied in two main experimental settings: in the first setting, mice were imaged immediately after vessel occlusion using a non-absorbable suture around one common carotid artery (CCA) or a sham surgery. In the second setting, the groups were imaged 1 week before (baseline) and 48 h after a transient occlusion (lasting 30 min) of one CCA or a sham surgery. Further experimental details are shown in the corresponding figures, Table 1, and “Supplementary Information.” PTX (150 μg/kg b.w., i.p.) or PBS were injected 48 h before surgery.

### Longitudinal Multiparametric MRI—Acquisitions and Analysis

Multiparametric MRI acquisitions were performed using a ClinScan 7-T small-animal MR scanner, a rat whole-body transmitting coil, and a 4-channel mouse brain surface receiving coil (Bruker Biospin). The imaging protocol consisted of anatomical T2-weighted images (T2WI), diffusion-weighted images (DWI), perfusion-weighted images (PWI), and multi-turbo-spin-echo T2-weighted acquisitions focusing specifically on the Bregma/Interaural 3.82 ± 0.25 mm brain region as

**Table 1** Summary of imaging experimental setup. The table shows the subdivisions of groups and time points. The number of animals used for statistics at every time point and animal group are displayed. Animals were injected with PTX 150 µg/kg b.w. i.p. or PBS 48 h before surgery. Images were obtained from mice in two main experimental

settings. One main group was imaged during occlusion or sham surgery (Top). The other main group was examined at baseline (BL) and 48 h after occlusion/reperfusion (unilateral transient CCA) or sham surgery (96 h)

Group name	<i>n</i>	PTX	Surgery	Image time point
Sham PBS	5	-	Sham	0 h
Sham PTX	4	+	Sham	0 h
Occlusion PBS	6	-	Occlusion	0 h
Occlusion PTX	5	+	Occlusion	0 h
Sham PBS	5	-	Sham	BL / 96 h
Sham PTX	4	+	Sham	BL / 96 h
Occlusion/reperfusion PBS	5	-	Occlusion/reperfusion	BL / 96 h
Occlusion/reperfusion PTX	4	+	Occlusion/reperfusion	BL / 96 h

previously performed [20–22] and detailed in the “Supplementary Information.”

### Volumes of Interest

All parametric images were coregistered to a common template using Pmod software (Bruker Biospin). Volumes of interest (VOIs) delimiting the striatal and cortical regions on both hemispheres were manually drawn at the above-described Bregma/Interaural brain regions using the T2WI as anatomical reference. The VOIs were overlaid on the PWI, ADC, and T2 maps followed by extraction of raw data. Lesion volumes were drawn on anatomical T2WI which covered the whole brain. Details are provided in the “Supplementary Information.”

### Single-Vessel Multi-gradient Echo (MGE) Imaging Experiment

We performed multi-gradient echo data acquisitions for single-vessel imaging using a 14.1 T / 26 cm magnet (MagneX, Oxford, UK) with an Avance III console (Bruker Biospin) and a 12-cm-diameter gradient providing 100G / cm with 150-µs rise time (Resonance Research, Massachusetts, U.S.A). A home-made RF surface coil (8-mm outer diameter) was used for single-vessel mapping. Details are provided in the “Supplementary Information.”

### Histology and Immunohistochemistry

For characterization of cerebral lesions, samples were stained with antibodies against CD31 (Abcam, Cambridge, UK), GFAP (Clone 6F2, Dako GmbH, Germany), HIF-1α (Clone ESEE 122, Abcam), and EPO (Clone H-162, Santa Cruz Biotechnology, Inc.). H&E staining was also

performed. Details are provided in the “Supplementary Information.”

### Statistics

Sample size and power calculations were conducted and approved by the local animal ethical committees. Animal numbers for the main experiments are shown in Table 1. We evaluated non-Gaussian distribution for all experimental datasets previous to statistical testing using the Jarque–Bera test. Whole-body perfusion data presented several datasets that were non-normality distributed; therefore, statistical evaluation was performed using a 2-sided non-parametric Wilcoxon signed-rank test. All other experiments were evaluated using either 2-way or 3-way ANOVA [25], followed by multiple comparison corrections using Tukey’s honestly significant test [26]. Details are provided in the “Supplementary Information.”

### Results

#### Differential Effects of a Functional Non-cerebral G<sub>i</sub>PCR KO on Blood Flow to Different Organs and Body Compartments

First, we examined the rough impact of PTX-induced functional non-cerebral G<sub>i</sub>PCR KO on blood flow in different organs and compartments using whole-body dynamic contrast-enhanced (DCE) MRI. ANOVA determined a statistically significant main group difference between PTX and control animals. To detect differences between the same organs of both groups, Wilcoxon matched-pairs signed-rank test was performed, and a statistically decreased blood flow was only found in the brain of PTX animals (Fig. 1A). As with some other organs and compartments, median blood flow in the ventricle, reflecting ejection fraction in this experimental setting, was lower than in the control group,

but without being statistically significant (Fig. 1B–F). Blood flow to the renal cortex after PTX treatment also suggested sustained perfusion of the kidney (Fig. 1C). The contrast agent accumulated in the renal calyceal system of PTX-treated animals, also indicating continued tubular excretion. The systemic results led us to investigate the effects of PTX in the brain using MRI techniques with better spatial resolution.

### Reduction of Global CBF Following Functional Systemic Non-cerebral G<sub>i</sub>PCR KO with PTX

To confirm and extend our observation of decreased CBF, we subjected the mice to an arterial spin labeling (ASL) MRI protocol (for details, see the “Materials and Methods” section and Fig. 2A, B), which shows the distribution of blood perfusion in the brain and provides reliable quantifications of CBF [21, 27, 28]. Coronal cross-sectional perfusion-weighted imaging (PWI) confirmed whole-brain hypoperfusion in PTX-pretreated sham-operated mice (Fig. 2C; yellow arrow). We quantified the CBF for the striatal and cortical regions (Fig. 2D, E). Both ipsi- and contralateral CBF were reduced by more than half in these regions compared to untreated sham-operated controls (Fig. 2D, E). Nevertheless, all of these reduced CBF values

were above a range associated with ischemic lesions [29, 30]. Thus, in agreement with the DCE measurements (see Fig. 1), our ASL data clearly reveal a systemic suppressive effect of PTX on CBF.

### PTX Administration Sensitizes to Ischemia

Having established that a functional non-cerebral G<sub>i</sub>PCR KO with PTX had an effect in CBF per se, we examined the consequences of acute occlusion of one common carotid artery (CCA) in cerebral hypoperfusion (see the “Materials and Methods” section and Fig. 2A, B). As evident from PWI, unilateral CCA occlusion in control animals treated with PBS resulted in a large decrease on CBF ipsilateral to the occlusion (Fig. 2C, Suppl. Fig. 1B; green arrow). This is also reflected in the calculated CBF values, which showed a clear hypoperfusion for the ipsilateral striatum and cortex (Fig. 2D). However, the hypoperfusion did not reach a level described to cause ischemia and necrosis [29, 30]. Of note, blood flow in the contralateral regions remained stable (Fig. 2E), which should allow for potential compensatory blood flow to the hypoperfused regions [31].

In contrast, PTX-pretreated mice showed global cerebral hypoperfusion that was further aggravated ipsilateral to the unilateral CCA ligation resulting in a complete breakdown of perfusion in both the striatum and cortex (Fig. 2C, D; Suppl. Fig. 1B; red arrow). These ipsilateral values were

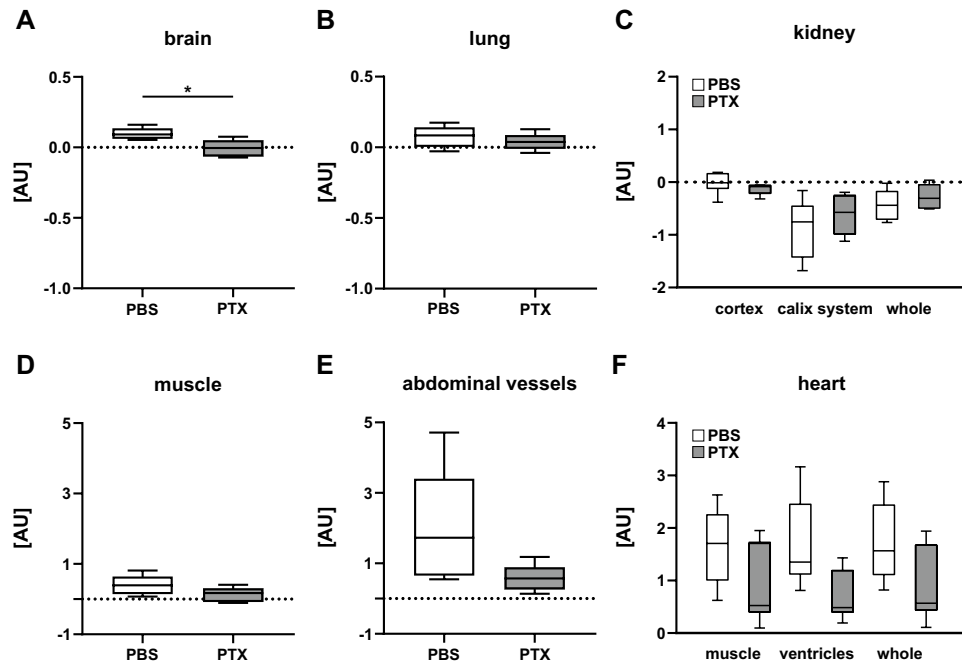


**Fig. 1** Functional non-cerebral G<sub>i</sub>PCR KO using PTX induces cerebral hypoperfusion. Whole-body perfusion was measured using dynamic contrast-enhanced imaging in PTX-pretreated and PBS-pretreated animals ( $n=5$  per group). **A** Wilcoxon matched-pairs signed-rank test found significant hypoperfusion in the brain of PTX-

injected mice in comparison to PBS-treated animals ( $* p < 0.05$ ). **B** Lung showed normal perfusion, whereas **C** kidney, **D** muscle, **E** abdominal vessels, and **F** heart yielded a hypoperfusion trend. Shown are median, 1st, and 3rd quartile of data distribution. The whiskers extend to the largest and smallest data point, respectively.

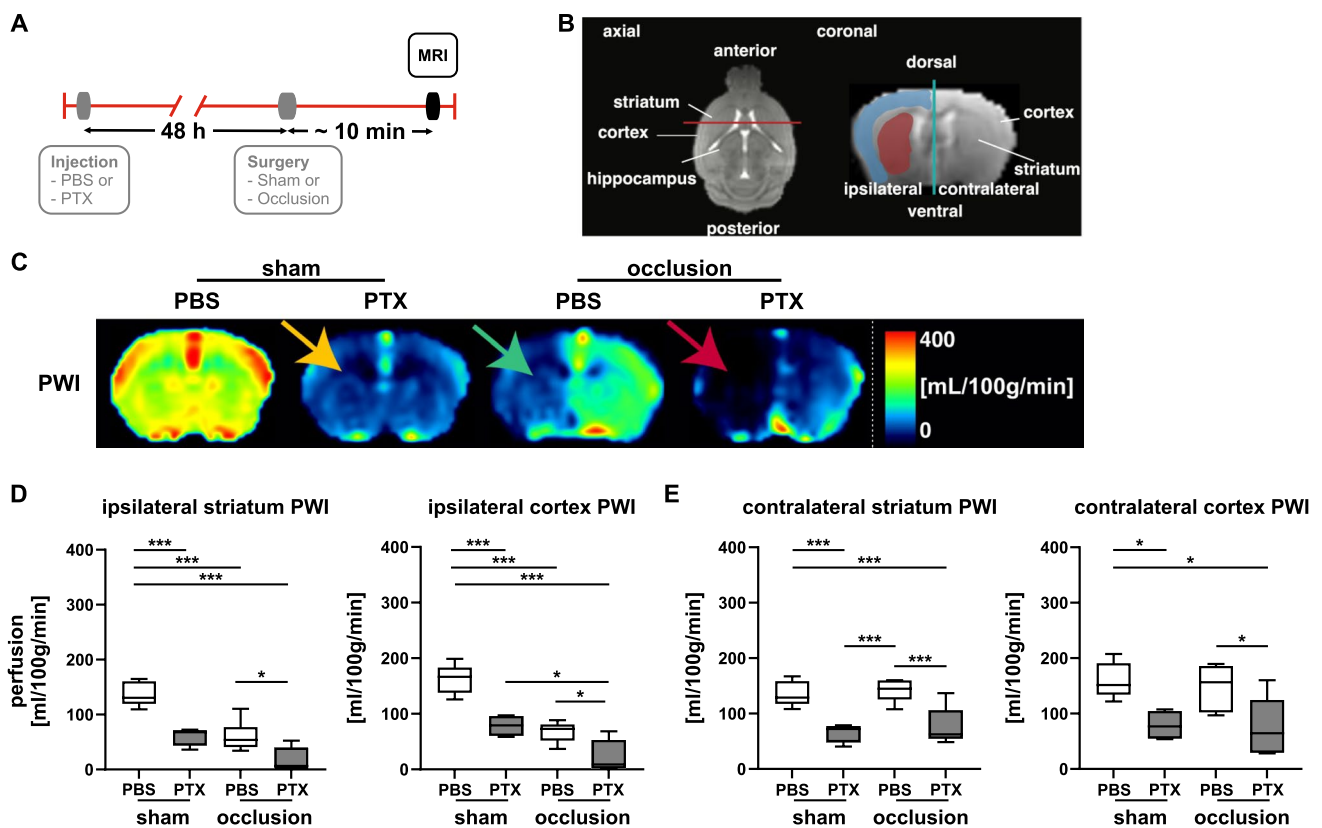


**Fig. 2** Functional PTX-induced non-cerebral  $G_i$ PCR KO sensitizes for cerebral ischemia during permanent carotid artery occlusion. **A** Timeline of PBS/PTX injection, surgery (sham or CCA occlusion), and arterial spin-labeling MRI analysis. **B** Schematic overview of axial and coronal cross-sections of the mouse brain. The different brain regions of interest used for analysis are indicated. The red line shows the position of the cross-section corresponding to the coronal view. The blue line depicts the limit of ipsi- and contra (right)-lateral brain hemispheres. **C** Perfusion-weighted images (PWI) indicate hypoperfusion of sham-operated PTX-treated mice (yellow arrow) compared to the sham PBS group. During left carotid artery ligation (occlusion), PBS-treated mice showed hypoperfusion visible in the ipsilateral hemisphere (green arrow), whereas PTX-

pretreated mice exhibited global cerebral hypoperfusion, confirming the effects observed in whole-body perfusion analysis. Moreover, the perfusion of PTX-pretreated mice was interrupted in the ipsilateral hemisphere (red arrow) during occlusion, in comparison to animals receiving PBS. Shown are images of one representative mouse per group. Further examples are provided in Suppl. Fig. 1B. Corresponding quantification and statistics of CBF are shown in **D** for ipsi- and **E** for contralateral striatum and cortex (for details see Table 1). Statistical analysis was performed using 2-way ANOVA (\*  $p < 0.05$ , \*\*\*  $p < 0.001$ ). Shown are median, 1st, and 3rd quartile of data distribution. The whiskers extend to the largest and smallest data point, respectively.

below the threshold at which ischemic injury occurs [29, 30]. On the contralateral side, an extent of reduction occurred that we had already observed in the sham-operated mice pretreated with PTX, and that may impede compensatory blood flow to the hypoperfused ipsilateral regions (Fig. 2E, Suppl. Fig. 1B).

Our findings show that a functional non-cerebral  $G_i$ PCR KO with PTX suppresses cerebral perfusion, which upon challenge by unilateral CCA occlusion severely disrupts CBF distal to the ligation, i.e., in the ipsilateral hemisphere. We were therefore interested in how perfusion subsequently developed and compared PWI at baseline and 48 h after surgery, which corresponded to 96 h after PTX administration (Suppl. Fig. 2A, B). The CBF in the brain of

the PBS-injected mice, sham-operated or transiently CCA-occluded, was invariant from baseline post surgically at 48 h (Suppl. Fig. 2C-F). The corresponding CBF in the non-cerebral  $G_i$ PCR KO mice was reduced albeit not significantly compared to baseline. Compared with the CBF of non-cerebral  $G_i$ PCR KO mice during occlusion (see Suppl. Fig. 1B and Fig. 2D, E) the CBF of mice monitored 48 h later, i.e., 96 h after PTX dosing (see Suppl. Fig. 2C-F), indicated a partial recovery. However, there was no difference in CBF in PTX-pretreated mice regardless of whether they were sham-operated or transiently CCA-occluded 48 h before (see Suppl. Fig. 2C-F). This finding was in contrast to the different results in the two PTX-pretreated groups, i.e., sham-operated or transiently CCA-occluded

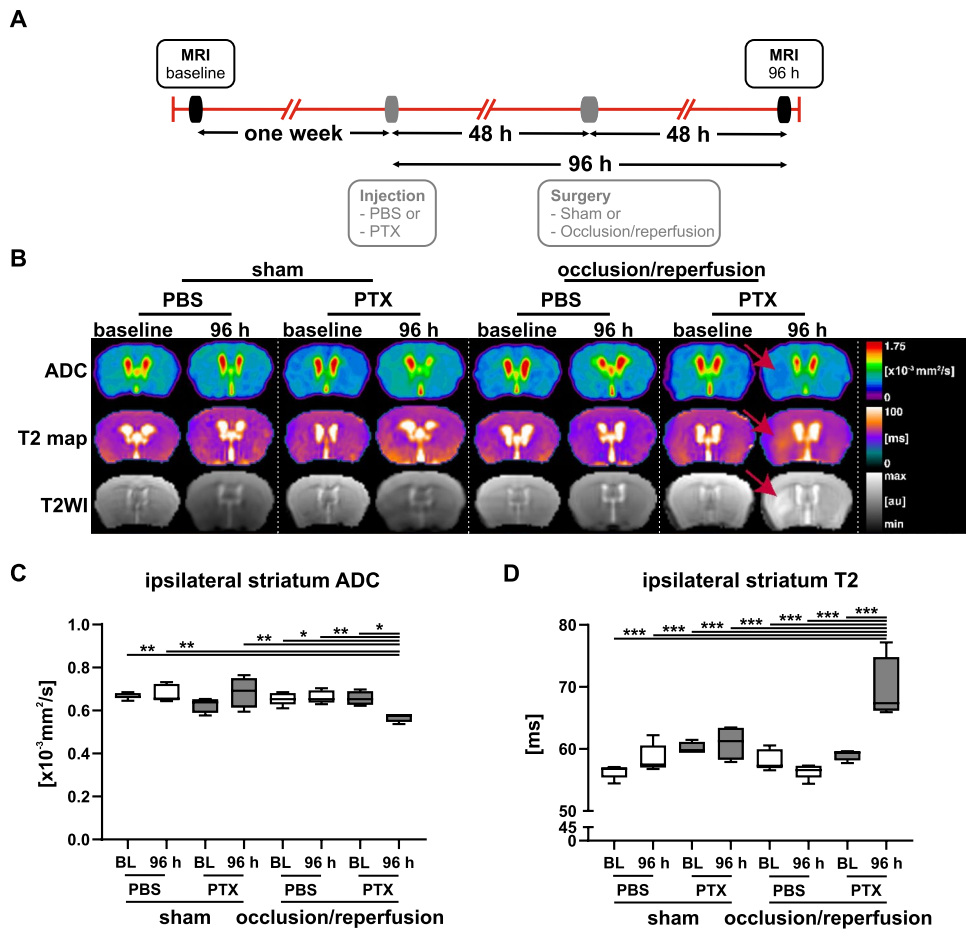


**Fig. 3** Cytotoxic and vasogenic edema in non-cerebral G<sub>1</sub>PCR KO following transient CCA occlusion. **A** Timeline of baseline MRI acquisition, PBS/PTX injection, surgery (sham or CCA occlusion), and post-operative MRI acquisitions. **B** Representative images of mouse brains showing the apparent diffusion coefficient (ADC), T2 map, and T2-weighted images (T2WI). Red arrows indicate the ischemic lesions in occluded PTX-pretreated mice consisting of reduced signal intensity of ADC images as well as hyperintensity in T2WI and T2 maps (for more details, see Tables 1, 2, and 3). Corre-

sponding quantification and statistical analysis of ipsilateral ADC (**C**) and T2 (**D**) in the striatum. Only PTX-pretreated mice following transient CCA occlusion presented a lesioned striatum with increments in ADC, accompanied by an increased T2 relaxation time. Statistical analysis was performed using 3-way ANOVA (\*  $p < 0.05$ , \*\*  $p < 0.01$ , \*\*\*  $p < 0.001$ ). Shown are median, 1st, and 3rd quartile of data distribution. The whiskers extend to the largest and smallest data point respectively.

**Table 2** Contralateral striatum results

Measurement (unit)	Group	BL	0 h	96 h
ADC ( $\times 10^{-3} \text{ mm}^2/\text{s}$ )	Sham PBS	0.66 ± 0.04	0.68 ± 0.15	0.68 ± 0.13
	Sham PTX	0.64 ± 0.08	0.62 ± 0.26	0.66 ± 0.15
	Occlusion PBS	0.65 ± 0.08	0.55 ± 0.13	0.65 ± 0.11
	Occlusion PTX	0.65 ± 0.08	0.62 ± 0.15	0.64 ± 0.08
T2 relaxation time (ms)	Sham PBS	56.7 ± 2.0	59.0 ± 3.4	58.7 ± 11.1
	Sham PTX	59.2 ± 2.4	55.6 ± 7.8	60.6 ± 5.5
	Occlusion PBS	61.0 ± 5.6	53.8 ± 3.6	56.8 ± 2.6
	Occlusion PTX	58.5 ± 3.8	56.2 ± 3.0	56.4 ± 2.4

**Table 3** Contralateral cortex results

Measurement (unit)	Group	BL	0 h	96 h
ADC ( $\times 10^{-3}$ mm <sup>2</sup> /s)	Sham PBS	0.65 $\pm$ 0.12	0.72 $\pm$ 0.20	0.65 $\pm$ 0.12
	Sham PTX	0.65 $\pm$ 0.15	0.65 $\pm$ 0.08	0.68 $\pm$ 0.15
	Occlusion PBS	0.66 $\pm$ 0.04	0.58 $\pm$ 0.23	0.67 $\pm$ 0.04
	Occlusion PTX	0.60 $\pm$ 0.06	0.60 $\pm$ 0.13	0.67 $\pm$ 0.06
T2 relaxation time (ms)	Sham PBS	59.8 $\pm$ 7.1	58.4 $\pm$ 4.0	59.9 $\pm$ 7.1
	Sham PTX	57.9 $\pm$ 4.7	57.8 $\pm$ 4.4	61.9 $\pm$ 4.7
	Occlusion PBS	59.6 $\pm$ 3.9	56.4 $\pm$ 4.4	59.6 $\pm$ 3.9
	Occlusion PTX	60.8 $\pm$ 1.6	57.0 $\pm$ 1.4	57.1 $\pm$ 1.6

at the time of occlusion (see Suppl. Fig. 1B and Fig. 2D, E). This prompted us to further investigate consequences of collapsed perfusion in non-cerebral G<sub>i</sub>PCR KO mice after transient unilateral CCA occlusion (Suppl. Fig. 3A).

### Functional Non-cerebral G<sub>i</sub>PCR KO Together with Transient Unilateral Carotid Artery Occlusion Leads to Cytotoxic and Vasogenic Edema

Diffusion-weighted images (DWI) provide a measurement of diffusion that can be quantified in the apparent diffusion coefficient (ADC) using MRI. ADC restrictions in the brain are the gold standard to identify ischemic stroke lesions, which have been shown to strongly correlate to final infarct lesions in tissue sections [32–35]. Diffusion restrictions have been known to start rapidly after stroke onset, peaking within one day, followed by slow value normalization [36, 37]. Consistent with these previous reports, PTX-pretreated and occluded mice already showed incipient ADC restrictions during occlusion (see Suppl. Fig. 3B–D), which were still evident in the mice imaged at 48 h post-surgery, corresponding to 96 h after PTX administration (Fig. 3B; red arrow, Fig. 3C). These ADC restrictions were clearly demarcated in DWIs of these mice (Suppl. Fig. 3B–D).

Moreover, T2 relaxation maps and T2WI representing vasogenic edema, demonstrated hyperintense signals only in the PTX-pretreated occluded animals at the latest timepoint (Fig. 3B, D; Suppl. Fig. 3B, E, F), consistent with previous literature [36, 37]. As the occluded animals pretreated with PTX showed vasogenic edema, we quantified edema volume in relation to their anatomical structures (Suppl. Fig. 4). In contrast, no signs of cytotoxic or vasogenic edema were detectable in both sham-operated groups and the PBS-treated occluded group 48 h after occlusion (Figs. 3C, D).

Because cytotoxic and vasogenic edema developed only in PTX-pretreated animals with transient CCA occlusion, we performed histological and immunohistochemical analyses to confirm the presence of an ischemic stroke phenotype, as we have previously done in other stroke models [20,

35]. Detection of ischemic lesions using hypoxia-inducible factor 1 $\alpha$  (HIF-1 $\alpha$ ) and erythropoietin (EPO) immunohistochemistry has been previously shown to clearly delimit the infarct core and the peri-infarct stroke region [38, 39] (Fig. 4A–D; Suppl. Fig. 5). The immunohistochemical staining showed focal lesions in the PTX-pretreated and CCA-occluded animals demonstrating ischemia ipsilateral to the occlusion, which perfectly colocalized with hyperintense lesions seen in DWIs and T2WIs (Fig. 4). Furthermore, H&E staining and immunohistochemistry for the endothelial markers CD31 and GFAP (Suppl. Fig. 5) revealed prominent lesions with neuronal pallor, vacuolation of the neuropil and edema (H&E) in various regions of the ipsilateral hemisphere, as well as blood vessels (CD31) and reactive gliosis (GFAP). Thus, clear signs of ischemic stroke through *in vivo* imaging were confirmed in PTX-pretreated transiently CCA-occluded animals using immunohistochemistry and histology.

### Functional Non-cerebral G<sub>i</sub>PCR KO with PTX Reduces Patency of Individual Cortex-Penetrating Microvessels

We investigated whether hypoperfusion was associated with collapsed microvessels. To specifically investigate the immediate response of microvessels to CCA occlusion, we used a multi-gradient echo (MGE) MRI sequence (Fig. 5A) [40–42]. High-resolution MGE-MRI provides a penetrating microvessel-specific measurement of the cortex that allows the estimation of microvascular collapse. Comparison of PBS-treated mice regardless of CCA occlusion revealed no difference in the number of vessels in both hemispheres (Fig. 5), indicating a normal microvascular function.

In contrast, the PTX-induced functional non-cerebral G<sub>i</sub>PCR KO provoked a reduction of quantifiable microvessels in the cortex of both hemispheres compared to the PBS groups (Fig. 5). The effect was further aggravated in the PTX-pretreated occluded mice, where an even more prominent number of microvessels collapsed in the ipsilateral

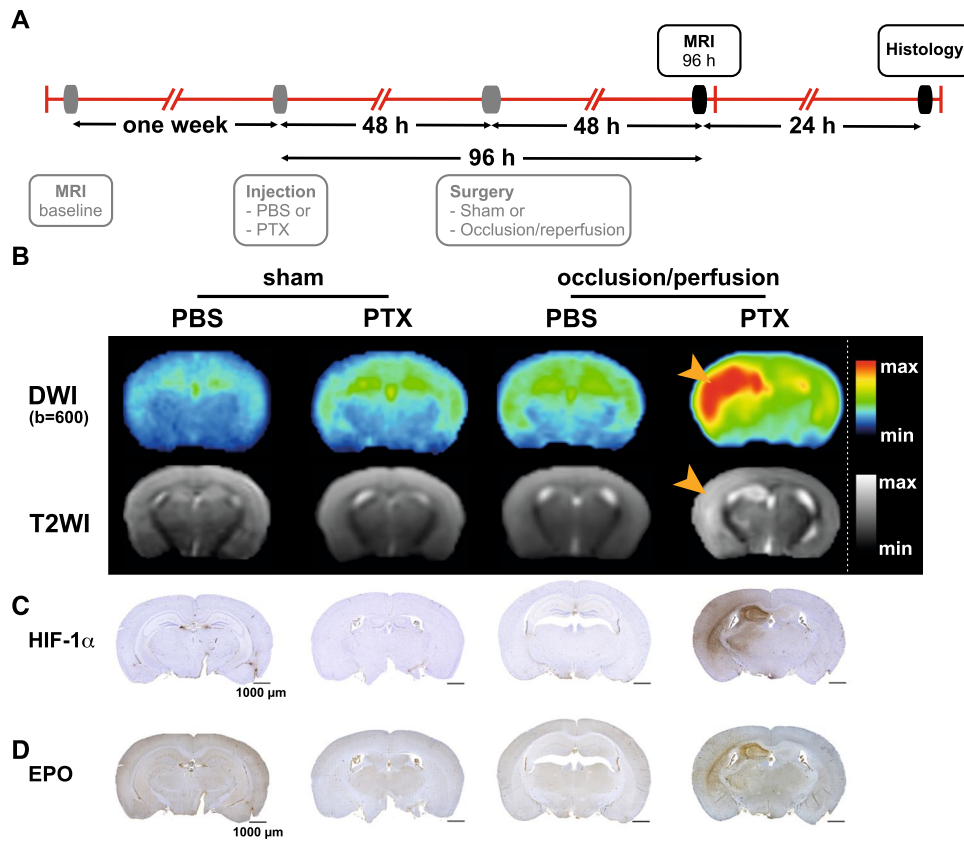


**Fig. 4** Colocalization of DWIs and T2WIs with immunohistochemical ischemia in occluded PTX-pretreated mice. **A** Timeline of PBS/PTX injection protocol, surgery, and MRI acquisition. **B** DWI ( $b$  value = 600 s/mm<sup>2</sup>) and T2WI of animals at 96 h on the coronal projection. The occluded PTX-pretreated mice show hyperintensities in the striatal, hippocampal, and cortical brain regions on DWI and T2WI (orange arrowheads). Animals of the other groups showed no

visible lesions. For more details, see Table 1. **C** HIF-1 $\alpha$  is stained in hippocampal stroke regions and marks the infarcted region colocalizing with the DWIs. **D**. Staining of the hypoxia-inducible cytokine EPO shows a focalized lesion similar to the HIF-1 $\alpha$ -positive hypoxic region further confirming an ischemic event. Immunohistochemistry was done in  $n=4$  mice per group.

cortex (Fig. 5). In combination with our perfusion experiments, these data suggest that PTX does not only cause global cerebral hypoperfusion but also micro-cerebrovascular collapse, which has also been described to occur under low-perfusion pressure in heart vessels [7].

## Discussion

Cerebrovascular functions of G<sub>i</sub>PCR-driven signaling are still largely unknown. To gain more insight, we employed the highly specific inhibitor PTX in order to specifically disrupt extraneuronal G<sub>i</sub>PCR signaling. Our results point to previously unrecognized functions of G<sub>i</sub>PCR signaling in the regulation of CBF and possibly systemic blood flow. Furthermore, extraneuronal functional PTX-induced non-cerebral G<sub>i</sub>PCR KO in combination with unilateral CCA produces brain lesions with similar imaging characteristics to human ischemic stroke.

One major drawback of the functional non-cerebral G<sub>i</sub>PCR KO with PTX is the ubiquitous nature of the KO in a multitude of systemic cellular processes. The systemic non-cerebral G<sub>i</sub>PCR KO may induce alterations in various systems, such as cardiovascular and immune system. In fact, it is used to establish the pertussis toxin-induced reversible encephalopathy dependent on monocyte chemoattractant protein-1 overexpression (PREMO) model, consisting on the injection of *Mycobacterium tuberculosis* and two injections of PTX [43]. We have previously shown that although PTX-sensitive G<sub>i</sub> proteins are ubiquitously expressed, a single extraneuronal application of the toxin *in vivo* does not modify neuronal G<sub>i</sub>PCR and does not cross through the intact BBB [19]. Therefore, it is possible under this specific setting, to evaluate the effects of PTX in the perfusion of brain vessels and in systemic perfusion, without unwanted effects in neurons. We evaluated systemic hemodynamic effects using whole-body perfusion in order to reveal major possible alterations, and although we found only significant effects in

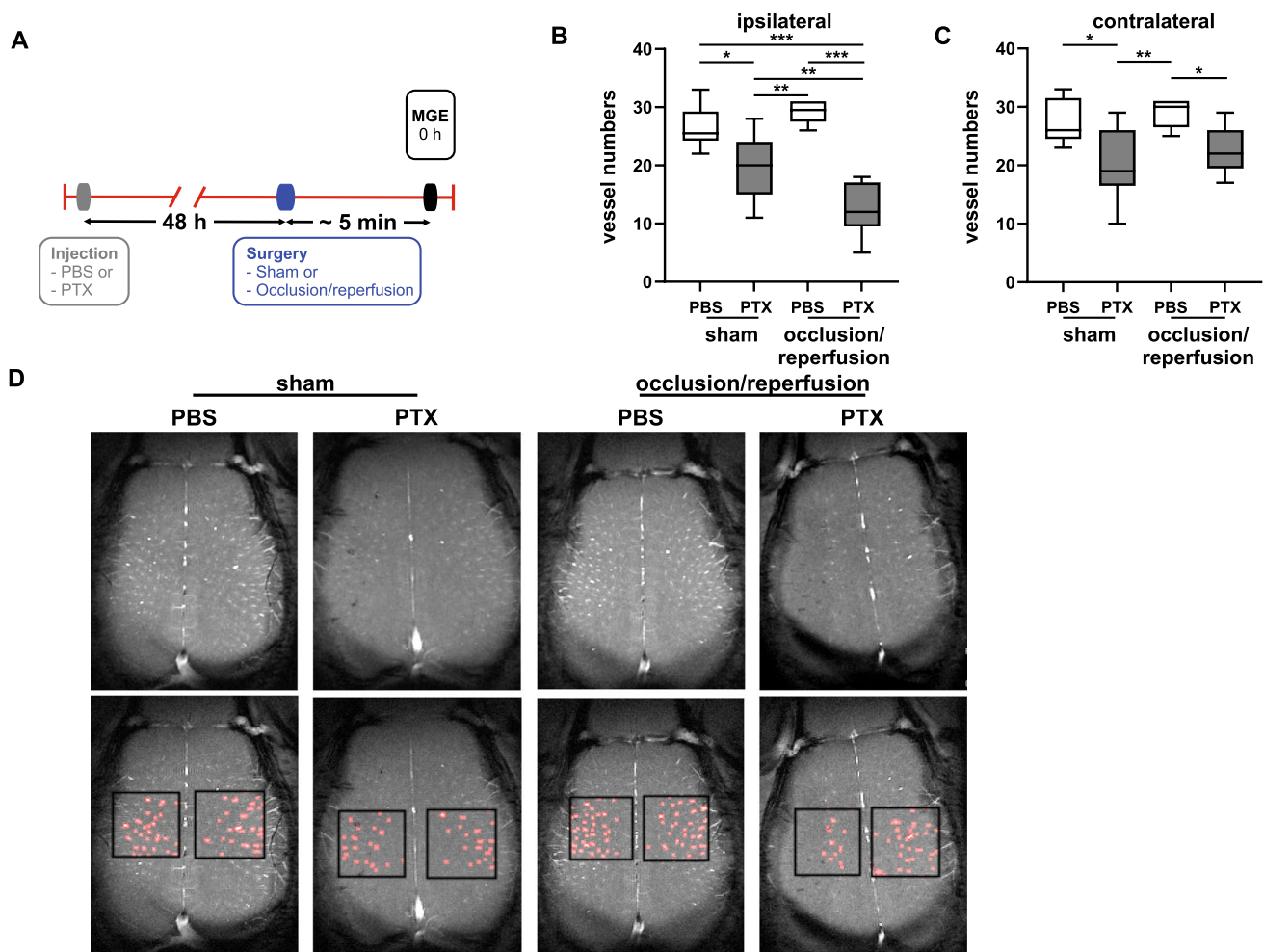


**Fig. 5** Functional non-cerebral  $G_1$ PCR KO reduces patency of cortex-penetrating microvessels. **A** Timeline of PBS/PTX injection and surgery protocol following multi-gradient echo (MGE) MRI acquisition. These experiments were performed during occlusion or sham surgery. Results of quantification of vessel numbers in the ipsi- (**B**) and (**C**) contralateral cortex ( $n=6-9$ ). Vessel numbers of PTX-pretreated mice are reduced in both hemispheres, which is further aggravated

upon occlusion in the ipsilateral cortex. Statistical analysis was performed using 2-way ANOVA (\*  $p < 0.05$ , \*\*  $p < 0.01$ , \*\*\*  $p < 0.001$ ). **D** Representative pictures from all four groups measured by MGE (upper panel). The black boxes mark the assessed areas, and the red dots are the identified vessels (lower panel). Shown are median, 1st, and 3rd quartile of data distribution. The whiskers extend to the largest and smallest data point, respectively.

the brain, other effects on systemic hemodynamics cannot be excluded. In fact, it has been demonstrated that PTX induces changes in blood pressure in hypertensive rats [2]. Moreover, it has been reported that in the cardiovascular system, PTX activity induces vessel size-dependent changes in vascular resistance [7], impairs endothelial  $Ca^{2+}$  influx [8], or lowers  $Ca^{2+}$  sensitivity of vasoconstriction in response to noradrenaline [2]. In line with these previous works, our findings now reveal a relevant effect in global cerebral hypoperfusion and microvascular collapse of cerebral vessels. The microvessel dysfunction could be at least partially mediated by interference with vascular  $G_i$  protein-mediated signaling affecting nitric oxide,  $\beta$ -adrenergic, angiotensin II type 1, serotonin-1A, or relaxin receptor function [2, 15, 18, 44]. Moreover, PTX has been shown to inhibit endothelium-dependent

relaxation in hypercholesterolemic and atherosclerotic arteries [15, 16], which specifically links a disrupted G protein-mediated transduction to microvascular dysfunction. Indeed, chronic hypertension, dyslipidemias, diabetes, and increased age have been correlated to hypoperfusion and microarterial impairment [45–47].

Interestingly, PTX has been recently reported to be neuroprotective due to a reduction of glutamate-induced calcium influx into ischemic neurons [48]. Tang et al. injected PTX as a neuroprotectant at a dose of 40  $\mu\text{g}/\text{kg}$  b.w. 30 min after applying a permanent middle cerebral artery occlusion. This occlusion triggered a BBB breakdown, allowing PTX to enter the brain [37, 49]. Consequently, Tang et al. injected PTX at a lower dose and at a time when the ischemic brain had a permeable BBB and could potentially benefit from inhibition of

calcium influx. However, no perfusion deficits were observed in this study. In the current study, we administered the toxin again at 150 µg/kg b.w. 48 h before carotid artery occlusion; thus, the BBB was intact at the moment of PTX injection and not able to reach the neurons [19]. The comparison of the work from Tang et al. to our study is an excellent reminder of how timing and dosage of therapeutic interventions, especially in niche compartments, are important for outcome.

The significance of our findings in the clinical field is directly related to the involvement of G protein signaling alterations in the pathogenesis of neurodegenerative and cerebrovascular diseases. G protein signaling is involved with neurotransmitters such as acetylcholine, GABA (gamma-aminobutyric acid), and glutamate. Here, for example, the acetylcholine receptor has been associated to formation of Aβ peptide and neurofibrillary tangles in Alzheimer's disease [50]. From a vascular perspective, alterations in G protein signaling involving monoamines such as adrenaline, noradrenaline, serotonin, dopamine, and histamine could be directly associated with cerebral hypoperfusion, a well-known imaging hallmark of neurodegenerative diseases [21, 51, 52]. Cerebral hypoperfusion is also a common risk factor in cerebrovascular diseases such as cerebral microbleeds and stroke [53, 54]. Therefore, G<sub>i</sub>PCR-driven signaling for the maintenance of CBF may be relevant to identify novel therapeutic targets. The PTX-triggered CBF impairment sensitized the brain to ischemic injury by disabling the mechanisms of blood flow regulation, an interesting effect that requires further mechanistic clarification focusing on the deficiency of specific G protein isoforms. The impaired hemodynamic stability and responsiveness of the cerebrovascular system caused by functional non-cerebral G<sub>i</sub>PCR KO in mice are reminiscent of observed hypoperfusion and vascular dysfunction in humans with chronic vascular disease, which is also predictive of human stroke severity [47].

Up to now, blocked GiPCR signaling had not yet been linked to the occurrence of cerebrovascular hypoperfusion and vascular collapse. It will be interesting to identify the specific G<sub>i</sub>PCRs involved in the maintenance of CBF and vascular tone. Furthermore, the effects of hypoperfusion and microvascular collapse induced by functional non-cerebral G<sub>i</sub>PCR KO may be useful for neuroscience, functional neuroimaging, and neurooncology.

**Supplementary Information** The online version contains supplementary material available at <https://doi.org/10.1007/s11307-022-01764-8>.

**Acknowledgements** Special thanks to Dr. Lisa Wang for her expertise and advice on the statistical analyses performed for this manuscript. The authors thank Daniel Bukala, Maren Harant, Henri De Maissin, Sandra Schwegmann, and Dennis Thiele for their assistance in this research. We are indebted to Prof. Klaus Schulze-Osthoff for valuable comments and discussions.

**Author Contribution** S.C.V., S.B.-H., B.J.P., B.N. designed research; S.C.V., S.B.-H., H.N., M.V., H.Z., Y.H., U.F., U.K., I.G.M., X.Y. performed research; S.C.V., A.M.S., J.-M.H. contributed reagents/analytic tools; S.C.V., M.V., A.M.S., V.L., I.G.M., L.Q.-M., X.Y., B.J.P., B.N. analyzed data; and S.C.V., S.B.-H., V.L., M.G., X.Y., B.J.P., B.N. wrote the paper. All authors read and edited the paper.

**Funding** Open Access funding enabled and organized by Projekt DEAL. Funding for this research project was provided by the DFG (to B.N.: GRK 1089, SFB 612, NU 53/12–2; NU 53/13–1; to X.Y.: YU 215/3–1, to M.G. GRK 1365, GO 766/12–3, GO 766/15–2, GO 766/18–2), BMBF (to X.Y.: 01GQ1702), NIH Brain Initiative (to X.Y.: 1RF1NS113278-01), the Werner-Siemens foundation (to B.P.), and Karl Kuhn foundation (to B.N.).

## Declarations

**Conflict of Interest** The authors declare no competing interests.

**Open Access** This article is licensed under a Creative Commons Attribution 4.0 International License, which permits use, sharing, adaptation, distribution and reproduction in any medium or format, as long as you give appropriate credit to the original author(s) and the source, provide a link to the Creative Commons licence, and indicate if changes were made. The images or other third party material in this article are included in the article's Creative Commons licence, unless indicated otherwise in a credit line to the material. If material is not included in the article's Creative Commons licence and your intended use is not permitted by statutory regulation or exceeds the permitted use, you will need to obtain permission directly from the copyright holder. To view a copy of this licence, visit <http://creativecommons.org/licenses/by/4.0/>.

## References

- Nagata K, Ye C, Jain M et al (2000) G $\alpha$ 2 but not G $\alpha$ 3 is required for muscarinic inhibition of contractility and calcium currents in adult cardiomyocytes. *Circ Res* 87:903–909. <https://doi.org/10.1161/01.RES.87.10.903>
- Zemanciková A, Török J, Zicha J, Kunes J (2008) Inactivation of G(i) proteins by pertussis toxin diminishes the effectiveness of adrenergic stimuli in conduit arteries from spontaneously hypertensive rats. *Physiol Res* 57:299–302
- Hu K, Nattel S (1995) Mechanisms of ischemic preconditioning in rat hearts. *Circulation* 92:2259–2265. <https://doi.org/10.1161/01.CIR.92.8.2259>
- Rosenbaum DM, Rasmussen SGF, Kobilka BK (2009) The structure and function of G-protein-coupled receptors. *Nature* 459:356–363. <https://doi.org/10.1038/nature08144>
- Drake MT, Shenoy SK, Lefkowitz RJ (2006) Trafficking of G protein-coupled receptors. *Circ Res* 99:570–582. <https://doi.org/10.1161/01.RES.0000242563.47507.ce>
- Gohla A, Klement K, Piekorz RP et al (2007) An obligatory requirement for the heterotrimeric G protein G $\beta$ 3 in the autophagic action of insulin in the liver. *Proc Natl Acad Sci U S A* 104:3003–3008. <https://doi.org/10.1073/pnas.0611434104>
- Komaru T, Wang Y, Akai K et al (1994) Pertussis toxin-sensitive G protein mediates coronary microvascular control during autoregulation and ischemia in canine heart. *Circ Res* 75:556–566. <https://doi.org/10.1161/01.RES.75.3.556>
- Spitzbarth-Régnigny E, Petitcolin MA, Bueb JL et al (2000) Pertussis toxin-sensitive G $\beta$ 3-proteins and intracellular calcium sensitivity of vasoconstriction in the intact rat tail artery. *Br J Pharmacol* 131:1337–1344. <https://doi.org/10.1038/sj.bjp.0703703>

9. Nürnberg B (2000) Pertussis toxin as a pharmacological tool. In: Aktories K, Just I (eds) *Bact. Protein Toxins. Pertussis Toxin as a Pharmacological Tool*. (HEP, Vol. 145, Springer Berlin Heidelberg, Berlin, Heidelberg, pp 187–206. [https://doi.org/10.1007/978-3-662-05971-5\\_9](https://doi.org/10.1007/978-3-662-05971-5_9)
10. Regard JB, Kataoka H, Cano DA et al (2007) Probing cell type-specific functions of Gi *in vivo* identifies GPCR regulators of insulin secretion. *J Clin Invest* 117:4034–4043. <https://doi.org/10.1172/JCI32994>
11. Wang L, Pydi SP, Zhu L et al (2020) Adipocyte Gi signaling is essential for maintaining whole-body glucose homeostasis and insulin sensitivity. *Nat Commun* 11:1–17. <https://doi.org/10.1038/s41467-020-16756-x>
12. Lu C, Pelech S, Zhang H et al (2008) Pertussis toxin induces angiogenesis in brain microvascular endothelial cells. *J Neurosci Res* 86:2624–2640. <https://doi.org/10.1002/jnr.21716>
13. Kost CK Jr, Herzer WA, Li PJ, Jackson EK (1999) Pertussis toxin-insensitive G-proteins and regulation of blood pressure in the spontaneously hypertensive rat. *Clin Exp Pharmacol Physiol* 26:449–455. <https://doi.org/10.1046/j.1440-1681.1999.03058.x>
14. Li Y, Anand-Srivastava MB (2002) Inactivation of enhanced expression of G i proteins by pertussis toxin attenuates the development of high blood pressure in spontaneously hypertensive rats. *Circ Res* 91:247–254. <https://doi.org/10.1161/01.RES.0000029969.39875.4B>
15. Shimokawa H, Flavahan NA, Vanhoutte PM (1991) Loss of endothelial pertussis toxin-sensitive G protein function in atherosclerotic porcine coronary arteries. *Circulation* 83:652–660. <https://doi.org/10.1161/01.CIR.83.2.652>
16. Flavahan NA (1992) Atherosclerosis or lipoprotein-induced endothelial dysfunction: Potential mechanisms underlying reduction in EDRF/nitric oxide activity. *Circulation* 85:1927–1938. <https://doi.org/10.1161/01.CIR.85.5.1927>
17. Rao BD, Sarkar P, Chattopadhyay A (2020) Selectivity in agonist and antagonist binding to serotonin 1a receptors via G-protein coupling. *Biochim Biophys Acta - Biomembr* 1862:183265. <https://doi.org/10.1016/j.bbame.2020.183265>
18. Lian X, Beer-Hammer S, König GM et al (2018) RXFP1 receptor activation by relaxin-2 induces vascular relaxation in mice via a G $\alpha$ 2-protein/PI3K $\beta$ /nitric oxide-coupled pathway. *Front Physiol* 9:1–13. <https://doi.org/10.3389/fphys.2018.01234>
19. Castaneda Vega S, Leiss V, Piekorz R et al (2020) Selective protection of murine cerebral Gi/o-proteins from inactivation by parenterally injected pertussis toxin. *J Mol Med* 98:97–110. <https://doi.org/10.1007/s00109-019-01854-1>
20. Castaneda Vega S, Weint C, Calaminus C et al (2017) Characterization of a novel murine model for spontaneous hemorrhagic stroke using *in vivo* PET and MR multiparametric imaging. *Neuroimage* 155:245–256. <https://doi.org/10.1016/j.neuroimage.2017.04.071>
21. Maier FC, Wehrl HF, Schmid AM et al (2014) Longitudinal PET-MRI reveals  $\beta$ -amyloid deposition and rCBF dynamics and connects vascular amyloidosis to quantitative loss of perfusion. *Nat Med* 20:1485–1492. <https://doi.org/10.1038/nm.3734>
22. Weint C, Castaneda Vega S, Riehle H et al (2015) Endothelial depletion of murine SRF/MRTF provokes intracerebral hemorrhagic stroke. *Proc Natl Acad Sci* 112:9914–9919. <https://doi.org/10.1073/pnas.1509047112>
23. Devanathan V, Hagedorn I, Köhler D et al (2015) Platelet G $\alpha$ 2 protein G $\alpha$ 2 is an essential mediator of thrombo-inflammatory organ damage in mice. *Proc Natl Acad Sci* 112:6491–6496. <https://doi.org/10.1073/pnas.1505887112>
24. Köhler D, Devanathan V, de Oliveira B, Franz C et al (2014) G $\alpha$ 2 and G $\alpha$ 3-deficient mice display opposite severity of myocardial ischemia reperfusion injury. *PLoS ONE* 9:e98325. <https://doi.org/10.1371/journal.pone.0098325>
25. Khan A, Rayner G (2003) Robustness to non-normality of common tests for the many-sample location problem. *J Appl Math Decis Sci* 7:187–206. [https://doi.org/10.1207/S15327612JAMD0704\\_1](https://doi.org/10.1207/S15327612JAMD0704_1)
26. Nanda A, Mohapatra DBB, Mahapatra APK et al (2021) Multiple comparison test by Tukey's honestly significant difference (HSD): do the confident level control type I error. *Int J Stat Appl Math* 6:59–65. <https://doi.org/10.22271/math.2021.v6.i1a.636>
27. Bokkers RPH, Hernandez DA, Merino JG et al (2012) Whole-brain arterial spin labeling perfusion mri in patients with acute stroke. *Stroke* 43:1290–1294. <https://doi.org/10.1161/STROKEAHA.110.589234>
28. Zhang K, Herzog H, Mauler J et al (2014) Comparison of cerebral blood flow acquired by simultaneous [15O]water positron emission tomography and arterial spin labeling magnetic resonance imaging. *J Cereb blood flow Metab* 34:1373–1380. <https://doi.org/10.1038/jcbfm.2014.92>
29. Markus HS (2004) Cerebral perfusion and stroke. *J Neurol Neurosurg Psychiatry* 75:353–361. <https://doi.org/10.1136/jnnp.2003.025825>
30. Heiss W-D (2011) The ischemic penumbra: correlates in imaging and implications for treatment of ischemic stroke. *Cerebrovasc Dis* 32:307–320. <https://doi.org/10.1159/000330462>
31. Guo H, Itoh Y, Toriumi H et al (2011) Capillary remodeling and collateral growth without angiogenesis after unilateral common carotid artery occlusion in mice. *Microcirculation* 18:221–227. <https://doi.org/10.1111/j.1549-8719.2011.00081.x>
32. Benveniste H, Hedlund LW, Johnson GA (1992) Mechanism of detection of acute cerebral ischemia in rats by diffusion-weighted magnetic resonance microscopy. *Stroke* 23:746–754. <https://doi.org/10.1161/01.STR.23.5.746>
33. Shereen A, Nemkul N, Yang D et al (2011) Ex vivo diffusion tensor imaging and neuropathological correlation in a murine model of hypoxia-ischemia-induced thrombotic stroke. *J Cereb Blood Flow Metab* 31:1155–1169. <https://doi.org/10.1038/jcbfm.2010.212>
34. Zille M, Farr TD, Przesdzing I et al (2012) Visualizing cell death in experimental focal cerebral ischemia: promises, problems, and perspectives. *J Cereb Blood Flow Metab* 32:213–231. <https://doi.org/10.1038/jcbfm.2011.150>
35. Castaneda-Vega S, Katiyar P, Russo F et al (2021) Machine learning identifies stroke features between species. *Theranostics* 11:3017–3034. <https://doi.org/10.7150/thno.51887>
36. Loubinoux I, Volk A, Borredon J et al (1997) Spreading of vasogenic edema and cytotoxic edema assessed by quantitative diffusion and T2 magnetic resonance imaging. *Stroke* 28:419–427. <https://doi.org/10.1161/01.STR.28.2.419>
37. Jiang X, Andjelkovic AV, Zhu L et al (2018) Blood-brain barrier dysfunction and recovery after ischemic stroke. *Prog Neurobiol* 163–164:144–171. <https://doi.org/10.1016/j.pneurobio.2017.10.001>
38. Sirén A-L, Knerlich F, Poser W et al (2001) Erythropoietin and erythropoietin receptor in human ischemic/hypoxic brain. *Acta Neuropathol* 101:271–276. <https://doi.org/10.1007/s004010000297>
39. Wang GL, Jiang BH, Rue EA, Semenza GL (1995) Hypoxia-inducible factor 1 is a basic-helix-loop-helix-PAS heterodimer regulated by cellular O2 tension. *Proc Natl Acad Sci* 92:5510–5514. <https://doi.org/10.1073/pnas.92.12.5510>
40. Yu X, He Y, Wang M et al (2016) Sensory and optogenetically driven single-vessel fMRI. *Nat Methods* 13:337–340. <https://doi.org/10.1038/nmeth.3765>
41. He Y, Wang M, Chen X et al (2018) Ultra-slow single-vessel BOLD and CBV-based fMRI spatiotemporal dynamics and their correlation with neuronal intracellular calcium signals. *Neuron* 97:925–939.e5. <https://doi.org/10.1016/j.neuron.2018.01.025>
42. He Y, Wang M, Yu X (2020) High spatiotemporal vessel-specific hemodynamic mapping with multi-echo single-vessel fMRI. *J Cereb Blood Flow Metab* 40:2098–2114. <https://doi.org/10.1177/0271678X19886240>
43. Huang D, Tani M, Wang J et al (2002) Pertussis toxin-induced reversible encephalopathy dependent on monocyte chemoattractant

- protein-1 overexpression in mice. *J Neurosci* 22:10633–10642. <https://doi.org/10.1523/JNEUROSCI.22-24-10633.2002>
44. Hare JM, Kim B, Flavahan NA et al (1998) Pertussis toxin-sensitive G proteins influence nitric oxide synthase III activity and protein levels in rat heart. *J Clin Invest* 101:1424–1431. <https://doi.org/10.1172/JCI1012>
45. Yonas H, Smith HA, Durham SR et al (1993) Increased stroke risk predicted by compromised cerebral blood flow reactivity. *J Neurosurg* 79:483–489. <https://doi.org/10.3171/jns.1993.79.4.0483>
46. Isozaki M, Arai Y, Kudo T et al (2010) Clinical implication and prognosis of normal baseline cerebral blood flow with impaired vascular reserve in patients with major cerebral artery occlusive disease. *Ann Nucl Med* 24:371–377. <https://doi.org/10.1007/s12149-010-0367-9>
47. Gupta A, Chazen JL, Hartman M et al (2012) Cerebrovascular reserve and stroke risk in patients with carotid stenosis or occlusion. *Stroke* 43:2884–2891. <https://doi.org/10.1161/STROKEAHA.112.663716>
48. Tang Z, Li S, Han P et al (2015) Pertussis toxin reduces calcium influx to protect ischemic stroke in a middle cerebral artery occlusion model. *J Neurochem* 135:998–1006. <https://doi.org/10.1111/jnc.13359>
49. Abdullahi W, Tripathi D, Ronaldson PT (2018) Blood-brain barrier dysfunction in ischemic stroke: targeting tight junctions and transporters for vascular protection. *Am J Physiol Physiol* 315:C343–C356. <https://doi.org/10.1152/ajpcell.00095.2018>
50. Barrantes FJ, Borroni V, Vallés S (2010) Neuronal nicotinic acetylcholine receptor-cholesterol crosstalk in Alzheimer's disease. *FEBS Lett* 584:1856–1863. <https://doi.org/10.1016/j.febslet.2009.11.036>
51. Fernández-Seara MA, Mengual E, Vidorreta M et al (2012) Cortical hypoperfusion in Parkinson's disease assessed using arterial spin labeled perfusion MRI. *Neuroimage* 59:2743–2750. <https://doi.org/10.1016/j.neuroimage.2011.10.033>
52. Austin BP, Nair VA, Meier TB et al (2011) Effects of hypoperfusion in Alzheimer's disease. *Adv Alzheimer's Dis* 2:253–263. <https://doi.org/10.3233/978-1-60750-793-2-253>
53. Sweet JG, Chan S, Cipolla MJ (2015) Effect of hypertension and carotid occlusion on brain parenchymal arteriole structure and reactivity. *J Appl Physiol* 119:817–823. <https://doi.org/10.1152/jappphysiol.00467.2015>
54. Tian G, Ji Z, Lin Z et al (2020) Cerebral autoregulation is heterogeneous in different stroke mechanism of ischemic stroke caused by intracranial atherosclerotic stenosis. *Brain Behav* 11:1–13. <https://doi.org/10.1002/brb3.1907>

**Publisher's Note** Springer Nature remains neutral with regard to jurisdictional claims in published maps and institutional affiliations.